

1 **Deciphering autoantibody landscape of systemic sclerosis through systems-based**

2 **approach: insights from a B-cell depletion clinical trial**

3

4 Kazuki M Matsuda, MD, PhD,¹ Satoshi Ebata, MD, PhD,¹ Kazuhiro Iwadoh, MD,

5 PhD,¹ Hirohito Kotani, MD, PhD,¹ Teruyoshi Hisamoto, MD, PhD,¹ Ai Kuzumi, MD,

6 PhD,¹ Takemichi Fukasawa MD, PhD,^{1,2} Asako Yoshizaki-Ogawa, MD, PhD,¹ Shinichi

7 Sato, MD, PhD,¹ Ayumi Yoshizaki, MD, PhD^{1,2#}

8

9 1. Department of Dermatology, The University of Tokyo Graduate School of Medicine,

10 Tokyo, Japan

11 2. Department of Clinical Cannabinoid Research, The University of Tokyo Graduate

12 School of Medicine, Tokyo, Japan

13

14 **# Corresponding author**

15 Ayumi Yoshizaki, MD, PhD

16 Department of Dermatology and Department of Clinical Cannabinoid Research, The

17 University of Tokyo Graduate School of Medicine, 7-3-1, Hongo, Bunkyo-ku, Tokyo,

18 Japan, 1138655

19 Phone: +81-3-3815-5411

20 ORCID: 0000-0002-8194-9140

21 E-mail: ayuyoshi@me.com

22 _____

23 **Abstract**

24 Systemic sclerosis (SSc) is a progressive fibrotic disorder with a high mortality
25 rate, characterized by extensive autoantibody production. Despite recent advancements,
26 effective treatments remain limited. Rituximab (RTX), a B-cell depleting agent, has
27 shown promise in clinical trials. The DESIRES trial highlighted the reduction in
28 modified Rodnan Skin Score (mRSS) and the association between serum
29 immunoglobulin levels and RTX responsiveness. We employed proteome-wide
30 autoantibody screening (PWAS) using wet protein arrays (WPAs) that display 13,455
31 human autoantigens to analyze serum samples from SSc patients in the DESIRES trial
32 and age- and sex-matched healthy controls (HCs). As a result, the sum of autoantibody
33 levels (SAL) was significantly higher in SSc patients compared to HCs. High
34 responders (HRs) to RTX showed a greater initial SAL and significant reductions
35 post-treatment, unlike low responders (LRs). Machine learning identified specific
36 autoantibodies linked to disease status, and 58 autoantibodies were identified as
37 clinically relevant. Some of those autoantibodies targeted membrane proteins including
38 G protein-coupled receptors, associated with better differentiation between HRs and
39 LRs. Our findings underscore the significance of autoantibodies in SSc pathogenesis
40 and their potential role in predicting RTX responsiveness. This comprehensive

41 autoantibody profiling could enhance diagnostic and therapeutic strategies, and

42 moreover, better understanding of the pathophysiology of SSc.

43

44 **Introduction**

45 Systemic sclerosis (SSc) is a progressive fibrotic disorder that affects both the
46 skin and internal organs.¹ Among connective tissue diseases, it has the poorest
47 prognosis, with an approximate 30% mortality rate within ten years.² Historically,
48 treatment options for SSc have been limited. While the exact cause of SSc remains
49 unclear, increasing evidence indicates that B cells play a significant role in the
50 pathogenesis.³⁻⁵ They contribute by producing autoantibodies, secreting unique
51 cytokines, and activating other immune cells. Reflecting this understanding, various
52 B-cell targeting therapeutic modalities, monoclonal antibodies,⁶⁻⁸ Bruton's tyrosine
53 kinase inhibitors,⁹ and chimeric antigen receptor (CAR) T-cell therapies,¹⁰⁻¹² are
54 emerging as promising treatments for SSc.

55 Rituximab (RTX) is a chimeric monoclonal antibody that depletes circulating
56 B cells by targeting the B-cell specific antigen CD20. Previously, we conducted a
57 double-blind, investigator-initiated, randomized, placebo-controlled trial, or the
58 DESIRES trial,¹³ which demonstrated significant superiority of RTX over placebo by
59 the absolute reduction of modified Rodnan Skin Score (mRSS) 24 weeks after initiation
60 of the study period. The open-label extension of this trial also revealed the long-term

61 efficacy and safety of RTX on SSc,¹⁴ as well as the association between decrease in
62 serum immunoglobulins and greater clinical response to RTX.¹⁵

63 The emergence of autoantibodies is a prominent feature of SSc, highlighting its
64 nature as an autoimmune disorder. Anti-nuclear antibodies (ANAs), detected through
65 indirect immunofluorescence on HEp-2 cells, are present in more than 90% of patients
66 with SSc.¹⁶ Several ANAs are specific to SSc or are closely associated with distinct
67 clinical subsets. For instance, anti-topoisomerase I antibodies (ATA) are strongly linked
68 to diffuse skin sclerosis and severe interstitial lung disease (ILD), while anti-centromere
69 antibodies (ACA) are primarily associated with limited skin and lung involvement.¹⁷
70 However, the pathogenicity of these ANAs is debated, as they cannot reach their targets
71 across the plasma and nuclear membranes *in vivo*. Additionally, the DESIRES trials
72 revealed that serum ATA levels did not decrease,^{13,14} indicating that the relationship
73 between serum immunoglobulin levels and responsiveness to RTX cannot be explained
74 by ATA levels.

75 Herein, we employed our original technique for proteome-wide autoantibody
76 screening (PWAS) using wet protein arrays (WPAs) that cover approximately 90% of
77 the human transcriptome.^{18,19} This technique has previously been used to develop
78 multiplex measurements for disease-related autoantibodies,^{20,21} identify clinically

79 relevant novel autoantibodies,^{22,23} and investigate inter- and intra-molecular epitope
80 spreading during the disease course. We applied PWAS to serum samples from SSc
81 patients who participated in the DESIRES trial, as well as sex- and age-matched healthy
82 controls (HCs). Our aim was to elucidate the autoantibody landscape in SSc and
83 investigate clusters of autoantibodies that contribute to the reduction of serum
84 immunoglobulin levels associated with a good response to RTX in SSc patients. This
85 research seeks to identify novel biomarkers and gain a better understanding of the
86 pathogenesis of SSc.

87 **Results**

88 *Subjects*

89 In the DESIRES trial (NCT04274257), a total of 56 individuals diagnosed with
90 SSc were evenly randomized into two groups: 28 received RTX and 28 received a
91 placebo.¹³ Serum samples were collected at the start and after 24 weeks of treatment
92 from participants who completed the term. These samples were reacted with WPAs for
93 PWAS (**Figure 1A**). After excluding samples that were not suitable for PWAS, such as
94 those containing anti-GST-tag antibodies, the study proceeded with 24 patients in the
95 RTX group and 21 patients in the placebo group. The baseline characteristics of the two
96 groups were comparable (**Table 1**). An equal number of age- and sex-matched healthy
97 controls (HCs) were also included in the study (**Figure 1B**).

98

99 *The sum of autoantibody levels*

100 We defined the sum of autoantibody levels (SAL) as the total serum
101 concentration of all autoantibodies assessed in our PWAS. SAL was significantly higher
102 in SSc patients compared to HCs at the baseline ($P < 0.0001$; **Figure 1C**). Subsequently,
103 we categorized the RTX treatment group into two subgroups based on their response to
104 treatment (**Figure 1D**): high responders (HRs; $n = 11$) and low responders (LRs; $n = 13$).

105 Initially, SAL was significantly greater in the HR group compared to the LR group ($P <$
106 0.05 ; **Figure 1E**). Additionally, SAL levels decreased significantly from week 0 to
107 week 24 in the HR group ($P < 0.05$), whereas changes in the LR group were not
108 statistically significant. This pattern persisted across all age groups (**Extended Figure**
109 **1A**). In contrast, serum levels of well-known SSc-related autoantibodies, including
110 anti-topoisomerase I antibodies (ATA), anti-centromere antibodies (ACA), and
111 anti-RNA polymerase III antibodies (ARA), did not follow this trend, as observed both
112 in clinical-standard ELISA tests (**Figure 1F**) and in our PWAS (**Extended Figure 1B**).

113

114 *Machine learning*

115 To determine which autoantibodies were driving the association between the
116 SAL and disease status, we firstly utilized nine machine learning frameworks. Notably,
117 Lasso regression, Ridge regression, SVM with normalization, XGBoost, and LightGBM
118 achieved an area under the receiver-operator characteristics curve (ROC-AUC)
119 exceeding 0.96, demonstrating an almost perfect ability to distinguish between SSc
120 patients and HCs (**Table 2**). We identified the top 10 features in these six models
121 (**Extended Figure 2A**), examined their inclusion relationships (**Extended Figure 2B**),
122 and explored the prevalence of highlighted autoantibodies across a broader range of

123 human disorders using the aUToAntiBody Comprehensive Database (UT-ABCD).²⁴
124 Most of these autoantibodies were found to be non-specifically elevated in various
125 pathological conditions, except for well-known SSc-specific autoantibodies such as
126 ATA and ARA (**Extended Figure 2C**). Attempts to distinguish between HRs and LR
127 based on pre-treatment autoantibody profiles did not yield satisfactory precision
128 (**Extended Table 1**).

129

130 *Investigating clinically relevant autoantibodies*

131 We next sought to identify autoantibodies significantly associated with the
132 clinical features of SSc using the trial data that included longitudinal changes. Initially,
133 we selected autoantibodies that were significantly elevated in SSc patients compared to
134 HCs at baseline (**Figure 2A**). Next, we chose autoantibodies that were significantly
135 higher in HRs compared to LR (s) (**Figure 2B**). Lastly, we focused on autoantibodies
136 whose serum concentrations significantly decreased from week 0 to week 24 in HRs
137 (**Figure 2C**). As a result, 58 autoantibodies were identified as candidates for clinically
138 relevant autoantibodies in SSc (**Figure 2D**). Principal component analysis (PCA)
139 indicated that these 58 autoantibodies appear to distinguish HRs at week 0 within the
140 dataset (**Figure 2E**). The sum of the serum levels of these autoantibodies displayed a

141 pattern like SAL, but in a more pronounced manner (**Figure 2F**). Consistently,
142 ROC-AUC analysis showed that these 58 autoantibodies provide better differentiation
143 between SSc patients and HCs compared to the complete autoantibody profile (**Figure**
144 **2G**), and moreover, distinguish between HRs and LRs with nearly perfect precision
145 (**Figure 2H**).

146

147 *Profiling candidate autoantibodies*

148 To explore the molecular features of the human proteins targeted by the
149 identified candidate autoantibodies, we conducted gene ontology enrichment analyses
150 utilizing Metascape.²⁵ Notably, whereas established SSc-related autoantibodies
151 primarily target intracellular antigens, our findings emphasized membrane proteins
152 associated with processes such as "import across plasma membrane" and "peptide G
153 protein-coupled receptors (GPCRs)" (**Figure 3A**). There were four autoantibodies
154 linked to each of the processes "import across plasma membrane" and "peptide GPCRs"
155 (**Figure 3B**). Autoantibodies associated with plasma membrane import included those
156 targeting presenilin 1 (PSEN1), solute carrier family 22 member 2 (SLC22A2), transient
157 receptor potential cation channel subfamily V member 5 (TRPV5), and solute carrier
158 family 46 member 1 (SLC46A1; **Figure 3C**). The group related to peptide GPCRs

159 comprised autoantibodies against chemokine receptor 8 (CCR8), formyl peptide
160 receptor 1 (FPR1), melanocortin 1 receptor (MC1R), and G protein-coupled receptor 63
161 (GPR63; **Figure 3E**). The associations between each autoantibody and the clinical
162 characteristics of SSc were detailed in **Figures 3D and 3F**. We also investigated the
163 distribution of these highlighted autoantibodies in a broader population, utilizing
164 UT-ABCD. As a result, all the items were not specific to SSc (**Extended Figure 3**).

165 The tissue specificity of the highlighted autoantigens was investigated using
166 publicly available databases. Analysis of multiple human tissues through bulk RNA
167 sequencing data from the Human Protein Atlas²⁶ revealed that *CCR8* and *FPR1* are
168 enriched in bone marrow and lymphoid tissues (**Extended Figure 4, A and B**).
169 Single-cell RNA sequencing data from the Tabula Sapiens project²⁷ showed that *CCR8*
170 expression is enhanced in regulatory T cells (Tregs; **Extended Figure 4C**), while *FPR1*
171 expression is elevated in neutrophils (**Extended Figure 4D**). Meanwhile, *MC1R*
172 expression appeared to be relatively ubiquitous across different tissues.

173

174 *Weighted correlation network analysis*

175 We utilized weighted correlated network analysis (WGCNA)²⁸ to delve deeper
176 into the correlations between autoantibodies in SSc. Our study included 135 specimens

177 from SSc patients at weeks 0 and 24, as well as HCs. We constructed a correlation
178 network for all autoantibodies evaluated in our PWAS and identified 57 distinct
179 modules (**Figure 4A**). The "turquoise" module, which contained ATA, also included
180 half of the candidate autoantibodies: anti-TRPV5, CCR8, MC1R, and GPR63
181 antibodies (**Figure 4B**). The "darkmagenta" module included ARA. The "tan" module
182 included ACA. The other candidate autoantibodies did not appear in either the
183 "darkmagenta" or "tan" modules. We also conducted gene ontology analyses on the
184 gene lists encoding proteins targeted by autoantibodies within these three modules
185 (**Extended Table 2**). The Enrichment score was the highest for "mitochondrion
186 organization" in the "turquoise" module (**Figure 4C**). The enrichment scores for
187 "regulation of cellular response to stress" were highest in the "turquoise" module,
188 moderate in the "darkmagenta" module, and lowest in the "tan" module. This pattern
189 aligns with the clinical severity associated with ATA, ARA, and ACA.

190 We also reviewed the associations between each module and clinical traits
191 (**Figure 4D**). The "turquoise" module was positively linked to ATA, a higher modified
192 Rodnan Skin Score (mRSS) – the primary endpoint of the DESIRES trial – as well as to
193 lower patient-reported quality of life, evidenced by higher Health Assessment
194 Questionnaire (HAQ) scores and lower 36-Item Short Form Health Survey (SF-36)

195 scores. The "darkmagenta" module was associated with ARA positivity and higher
196 forced vital capacity of the lungs, indicating a lower degree of ILD. The "tan" module
197 was correlated with the ACA profile but did not show any significant associations with
198 other clinical traits
199

200 Discussion

201 In this study, we applied our original PWAS technique subjecting serum
202 samples from SSc patients who participated in the DESIRES trial, along with sex and
203 age-matched HCs. Our findings revealed a significant elevation in the overall amount of
204 autoantibodies in SSc patients compared to HCs (**Figure 1**). We identified 58
205 autoantibodies as clinically relevant candidates in SSc, which showed a strong response
206 to B-cell depletion therapy (**Figure 2**). Gene ontology analysis highlighted
207 autoantibodies targeting membranous proteins, including transmembrane transporters
208 and GPCRs (**Figure 3**). Most of them were clustered in the same module identified by
209 WGCNA, which was significantly associated with ATA positivity, higher mRSS, and
210 lower patient-reported quality of life (**Figure 4**). We demonstrated the nearly perfect
211 distinction between SSc and HC samples achieved through machine learning (**Table 2**),
212 and SSc patients who show good response to RTX treatment engaging the clinically
213 relevant autoantibodies highlighted in our analyses (**Figure 2H**). These results
214 underscore the effectiveness of our integrating systems-based comprehensive
215 autoantibody screening and bioinformatic analyses, which could be called as
216 "autoantigenomics."²⁹

217 Our machine learning analysis confirmed the prominence of well-known
218 SSc-specific ANAs such as ATA and ARA (**Extended Figure 2**). However, these
219 autoantibodies did not exhibit longitudinal changes during the clinical trial nor
220 differences between HRs and LRs to RTX treatment (**Figure 1F and Extended Figure**
221 **1B**), consistent with our previous findings.^{13,14} In contrast, we observed that changes in
222 the overall levels of autoantibodies were significantly correlated with RTX efficacy
223 (**Figure 1, C and E**). This discrepancy led us to investigate autoantibodies that exhibit
224 significant associations with the time course and drug response to RTX therapy. While
225 predictive factors for RTX responsiveness have been limited to clinical indicators such
226 as CD19-positive cell counts, mRSS, and serum levels of SP-D,³⁰ the clinically relevant
227 autoantibodies we identified were able to discriminate between HRs and LRs with high
228 accuracy (**Figure 2H**). Interestingly, some of these autoantibodies targeted membranous
229 antigens (**Figure 3**), suggesting that they are not only useful as biomarkers but also
230 could play a direct role in the pathogenesis of SSc.

231 Accumulating evidence has unveiled the relevance of autoantibodies targeting
232 GPCRs in immune-related human disorders, including SSc.³¹⁻³³ Notably, previous
233 studies have indicated the relationship between GPCRs targeted by the candidate
234 autoantibodies and the pathogenesis of SSc. CCR8 is primarily expressed on Tregs

235 **(Extended Figure 4C)**, which suppress autoimmune responses.³⁴ CC Chemokine 1
236 (CCL1) acts as a chemoattractant, recruiting Tregs to peripheral tissues by binding to
237 CCR8.³⁵ While direct evidence linking the CCR8-CCL1 axis to SSc pathogenesis is
238 lacking, blocking CCR8 could exacerbate autoimmune responses in SSc by inhibiting
239 Treg homing to target tissues. FPR1, which is abundantly expressed on neutrophils
240 **(Extended Figure 4D)**, induces inflammation when bound by its cognate ligands.³⁶
241 One such endogenous agonist is N-formyl-methionine (fMet), a mitochondrial
242 protein-derived molecule that serves as a damage-associated molecular pattern.³⁷ Lurley
243 R et al. have shown in SSc, elevated serum fMet levels and fMet-induced activation of
244 neutrophils through FPR1-dependent mechanisms.³⁸ Consistent with these findings, our
245 enrichment analysis highlighted mitochondrion-associated antigens targeted by
246 autoantibodies in SSc **(Figure 4C)**, suggesting mitochondrial destruction, which has
247 also been reported in other autoimmune conditions such as systemic lupus
248 erythematosus and rheumatoid arthritis. MC1R is expressed on various cell types
249 **(Extended Figure 4B)**, including melanocytes, inflammatory cells, endothelial cells,³⁹
250 and skin fibroblasts from SSc patients.⁴⁰ Its endogenous ligand,
251 α -melanocyte-stimulating hormone, induces melanin production in melanocytes and
252 promotes anti-inflammatory responses, such as inhibition of nuclear factor- κ B and

253 suppression of pro-inflammatory cytokines.⁴¹ Kondo M et al. demonstrated that
254 dersimelagon (MT-7117), an oral MC1R agonist, has favorable effects on inflammation,
255 vascular dysfunction, and fibrosis, which are key pathologies in preclinical SSc
256 models.⁴² This prompted a phase 2 clinical trial to evaluate the efficacy and tolerability
257 of MT-7117 in patients with early, progressive diffuse cutaneous SSc (NCT04440592).
258 Collectively, accumulating experimental and clinical evidence suggests that modulating
259 these GPCRs, either through stimulation or blockade, could potentially alter SSc disease
260 severity.

261 Meanwhile, it is important to note that the serum levels of the candidate
262 autoantibodies we identified were relatively modest compared to conventional
263 SSc-specific autoantibodies like ATA (**Extended Figure 1B**). Moreover, the presence
264 of these candidate autoantibodies did not appear to be specific to SSc, as indicated by
265 data from UT-ABCD (**Extended Figure 3A and 3B**). These suggest that the
266 pathogenesis of SSc may not be attributed to a single unique autoantibody that shows
267 strong cross-reactivity with conventional SSc-specific autoantibodies, but rather to a
268 collaboration of multiple autoantibodies. This hypothesis aligns with several
269 observations that suggest that SSc is a multifactorial disease, involving a combination
270 of various autoantibodies and other factors rather than a single causative factor. First,

271 genome-wide association studies have not identified a single gene mutation strongly
272 linked to SSc.⁴³ Second, the disease concordance in twins is modest and similar
273 between monozygotic and dizygotic twins, further supporting the notion that SSc is not
274 caused only by genetic factors.⁴⁴ Finally, and most importantly, the clinical
275 manifestations of SSc are highly heterogeneous.¹

276 Alternatively, a cluster of several autoantibodies, with combinations that vary
277 among patients, might explain the heterogeneity of clinical manifestations in SSc.⁴⁵
278 Co-localization of ATA and candidate autoantibodies within the same module identified
279 by WGCNA, as well as the distribution of ATA, ARA, and ACA among different
280 modules (**Figure 4**), support this hypothesis. Such clustering of autoantibodies might
281 result from cross reaction with a single specific exogenous antigen such as viruses,^{46,47}
282 or intermolecular epitope spreading, a phenomenon we have recently demonstrated to
283 be involved in SSc progression using the same WPA system. Further research is needed
284 to unravel the relationships among these autoantibodies and their collective contribution
285 to SSc development. This research should include comparisons of structural similarity
286 and epitope mapping for the relevant antigens, and longitudinal serological monitoring
287 in each case. Understanding these interactions will be crucial for comprehensively

288 elucidating the mechanisms underlying the autoimmune aspect of SSc and potentially
289 identifying new therapeutic targets.

290 Our study has several notable strengths. Firstly, the data presented is derived
291 from a prospective, randomized, placebo-controlled clinical trial, which includes two
292 time points (before and after RTX therapy). This adherence to good clinical practice
293 ensures high data accuracy. Secondly, the use of the wheat-germ *in vitro* protein
294 synthesis system and the manipulation technique for WPAs enabled high-throughput
295 expression of a variety of human proteins, including membranous proteins, on a single
296 platform.¹⁸ As a result, our autoantibody measurement could encompass a wider range
297 of antigens at an almost proteome-wide level, allowing for the application of
298 omics-based bioinformatics approaches to interpret the data.²⁴ Meanwhile, one major
299 limitation is the lack of functional assays both *in vitro* and *in vivo*. Further investigation
300 is needed to determine whether the candidate autoantibodies we identified act as
301 agonists or antagonists to their target proteins, and whether they influence the
302 pathophysiology of SSc. Moreover, the value of autoantibodies we identified for
303 predicting treatment response to RTX should be validated in external cohorts in
304 real-world clinical settings.
305

306 **References**

- 307 1. Allanore, Y. *et al.* Systemic sclerosis. *Nat. Rev. Dis. Prim.* **1**, 1–21 (2015).
- 308 2. Rubio-Rivas, M., Royo, C., Simeón, C. P., Corbella, X. & Fonollosa, V.
- 309 Mortality and survival in systemic sclerosis: Systematic review and
- 310 meta-analysis. *Semin. Arthritis Rheum.* **44**, 208–219 (2014).
- 311 3. Hasegawa, M. *et al.* B-lymphocyte depletion reduces skin fibrosis and
- 312 autoimmunity in the tight-skin mouse model for systemic sclerosis. *Am. J. Pathol.*
- 313 **169**, 954–66 (2006).
- 314 4. Numajiri, H. *et al.* B Cell Depletion Inhibits Fibrosis via Suppression of
- 315 Profibrotic Macrophage Differentiation in a Mouse Model of Systemic Sclerosis.
- 316 *Arthritis Rheumatol.* **73**, 2086–2095 (2021).
- 317 5. Fukasawa, T. *et al.* Single-cell-level protein analysis revealing the roles of
- 318 autoantigen-reactive B lymphocytes in autoimmune disease and the murine
- 319 model. doi:10.7554/eLife.
- 320 6. Daoussis, D. *et al.* A multicenter, open-label, comparative study of B-cell
- 321 depletion therapy with Rituximab for systemic sclerosis-associated interstitial
- 322 lung disease. *Semin. Arthritis Rheum.* **46**, 625–631 (2017).

- 323 7. Sircar, G., Goswami, R. P., Sircar, D., Ghosh, A. & Ghosh, P. Intravenous
324 cyclophosphamide vs rituximab for the treatment of early diffuse scleroderma
325 lung disease: Open label, randomized, controlled trial. *Rheumatol. (United*
326 *Kingdom)* **57**, 2106–2113 (2018).
- 327 8. Ebata, S. *et al.* Rituximab therapy is more effective than cyclophosphamide
328 therapy for Japanese patients with anti-topoisomerase I-positive systemic
329 sclerosis-associated interstitial lung disease. *J. Dermatol.* **46**, 1006–1013 (2019).
- 330 9. Einhaus, J. *et al.* Inhibition of effector B cells by ibrutinib in systemic sclerosis.
331 *Arthritis Res. Ther.* **22**, 1–8 (2020).
- 332 10. Bergmann, C. *et al.* Treatment of a patient with severe systemic sclerosis (SSc)
333 using CD19-targeted CAR T cells. *Ann. Rheum. Dis.* **82**, 1117–1120 (2023).
- 334 11. Merkt, W. *et al.* Third-generation CD19.CAR-T cell-containing combination
335 therapy in Scl70+ systemic sclerosis. *Ann. Rheum. Dis.* **83**, 543 LP – 546 (2024).
- 336 12. Fabian, M. *et al.* CD19 CAR T-Cell Therapy in Autoimmune Disease — A Case
337 Series with Follow-up. *N. Engl. J. Med.* **390**, 687–700 (2024).
- 338 13. Ebata, S. *et al.* Safety and efficacy of rituximab in systemic sclerosis
339 (DESIREs): a double-blind, investigator-initiated, randomised,
340 placebo-controlled trial. *Lancet Rheumatol.* **3**, e489–e497 (2021).

- 341 14. Ebata, S. *et al.* Safety and efficacy of rituximab in systemic sclerosis
342 (DESIREs): open-label extension of a double-blind, investigators-initiated,
343 randomised, placebo-controlled trial. *Lancet Rheumatol.* **4**, e546–e555 (2022).
- 344 15. Kuzumi, A. *et al.* Long-term Outcomes After Rituximab Treatment for Patients
345 With Systemic Sclerosis: Follow-up of the DESIREs Trial With a Focus on
346 Serum Immunoglobulin Levels. *JAMA Dermatology* **159**, 374–383 (2023).
- 347 16. Okano, Y. Antinuclear antibody in systemic sclerosis (scleroderma). *Rheum Dis*
348 *Clin North Am* **22**, 709–35 (1996).
- 349 17. Nihtyanova, S. I. & Denton, C. P. Autoantibodies as predictive tools in systemic
350 sclerosis. *Nat. Rev. Rheumatol.* **6**, 112–116 (2010).
- 351 18. Goshima, N. *et al.* Human protein factory for converting the transcriptome into
352 an in vitro-expressed proteome. *Nat. Methods* **5**, 1011–1017 (2008).
- 353 19. Fukuda, E. *et al.* Identification and characterization of the antigen recognized by
354 the germ cell mAb TRA98 using a human comprehensive wet protein array.
355 *Genes to Cells* **26**, 180–189 (2021).
- 356 20. Matsuda, K. M. *et al.* Autoantibody Landscape Revealed by Wet Protein
357 Array: Sum of Autoantibody Levels Reflects Disease Status. *Front. Immunol.*
358 **13**, 1–14 (2022).

- 359 21. Kuzumi, A. *et al.* Comprehensive autoantibody profiling in systemic
360 autoimmunity by a highly-sensitive multiplex protein array. *Front. Immunol.* **14**,
361 (2023).
- 362 22. Matsuda, K. M., Kotani, H., Yamaguchi, K., Okumura, T. & Fukuda, E.
363 Significance of anti-transcobalamin receptor antibodies in cutaneous arteritis
364 revealed by proteome-wide autoantibody screening. *J. Autoimmun.* **135**, 102995
365 (2023).
- 366 23. Matsuda, K. M. *et al.* Autoantibodies to nuclear valosin-containing protein-like
367 protein: systemic sclerosis-specific antibodies revealed by in vitro human
368 proteome. *Rheumatology (Oxford)*. (2024) doi:10.1093/rheumatology/keae063.
- 369 24. Matsuda, K. M. *et al.* Proteome-wide autoantibody screening and holistic
370 autoantigenomic analysis unveil COVID-19 signature of autoantibody landscape.
371 *medRxiv* 2024.06.07.24308592 (2024) doi:10.1101/2024.06.07.24308592.
- 372 25. Zhou, Y. *et al.* Metascape provides a biologist-oriented resource for the analysis
373 of systems-level datasets. *Nat. Commun.* **10**, 1523 (2019).
- 374 26. Fagerberg, L. *et al.* Analysis of the human tissue-specific expression by
375 genome-wide integration of transcriptomics and antibody-based proteomics. *Mol.*
376 *Cell. Proteomics* **13**, 397–406 (2014).

- 377 27. The Tabula Sapiens Consortium. The Tabula Sapiens: A multiple-organ,
378 single-cell transcriptomic atlas of humans. *Science* (80-.). **376**, eabl4896 (2022).
- 379 28. Langfelder, P. & Horvath, S. WGCNA: An R package for weighted correlation
380 network analysis. *BMC Bioinformatics* **9**, (2008).
- 381 29. Moritz, C. P. *et al.* Autoantigenomics: Holistic characterization of autoantigen
382 repertoires for a better understanding of autoimmune diseases. *Autoimmun. Rev.*
383 **19**, 102450 (2020).
- 384 30. Matsuda, K. M. *et al.* Development of a prediction model of treatment response
385 in patients with cutaneous arteritis: Insights from a cohort of 33 patients. *J.*
386 *Dermatol.* **48**, 1021–1026 (2021).
- 387 31. Cabral-Marques, O. *et al.* GPCR-specific autoantibody signatures are associated
388 with physiological and pathological immune homeostasis. *Nat. Commun.* **9**, 5224
389 (2018).
- 390 32. Cabral-marques, O. *et al.* Autoantibodies targeting GPCRs and RAS-related
391 molecules associate with COVID-19 severity. *Nat. Commun.* **13**, 1220 (2022).
- 392 33. Akbarzadeh, R., Müller, A., Humrich, J. Y. & Riemekasten, G. When natural
393 antibodies become pathogenic: autoantibodies targeted against G

- 394 protein-coupled receptors in the pathogenesis of systemic sclerosis. *Front.*
395 *Immunol.* **14**, 1213804 (2023).
- 396 34. Barsheshet, Y. *et al.* CCR8+FOXP3+ Treg cells as master drivers of immune
397 regulation. *Proc. Natl. Acad. Sci.* **114**, 6086–6091 (2017).
- 398 35. Tiffany, H. L. *et al.* Identification of CCR8: a human monocyte and thymus
399 receptor for the CC chemokine I-309. *J. Exp. Med.* **186**, 165–170 (1997).
- 400 36. McDonald, B. *et al.* Intravascular Danger Signals Guide Neutrophils to Sites of
401 Sterile Inflammation. *Science (80-.)*. **330**, 362–367 (2011).
- 402 37. Zhang, Q. *et al.* Circulating mitochondrial DAMPs cause inflammatory responses
403 to injury. *Nature* **464**, 104–107 (2010).
- 404 38. Napolitano, F. *et al.* N-formyl peptide receptors induce radical oxygen
405 production in fibroblasts derived from systemic sclerosis by interacting with a
406 cleaved form of urokinase receptor. *Front. Immunol.* **9**, (2018).
- 407 39. Getting, S. J. Targeting melanocortin receptors as potential novel therapeutics.
408 *Pharmacol. Ther.* **111**, 1–15 (2006).
- 409 40. Kokot, A. *et al.* α -melanocyte-stimulating hormone suppresses
410 bleomycin-induced collagen synthesis and reduces tissue fibrosis in a mouse

- 411 model of scleroderma: Melanocortin peptides as a novel treatment strategy for
412 scleroderma? *Arthritis Rheum.* **60**, 592–603 (2009).
- 413 41. Wang, W., Guo, D.-Y., Lin, Y.-J. & Tao, Y.-X. Melanocortin Regulation of
414 Inflammation. *Front. Endocrinol. (Lausanne)*. **10**, (2019).
- 415 42. Kondo, M. *et al.* Dersimelagon, a novel oral melanocortin 1 receptor agonist,
416 demonstrates disease-modifying effects in preclinical models of systemic
417 sclerosis. *Arthritis Res. Ther.* **24**, 1–17 (2022).
- 418 43. Ishikawa, Y. *et al.* GWAS for systemic sclerosis identifies six novel
419 susceptibility loci including one in the Fc γ receptor region. *Nat. Commun.* **15**,
420 319 (2024).
- 421 44. Feghali-Bostwick, C., Medsger, T. A. J. & Wright, T. M. Analysis of systemic
422 sclerosis in twins reveals low concordance for disease and high concordance
423 for the presence of antinuclear antibodies. *Arthritis Rheum.* **48**, 1956–1963
424 (2003).
- 425 45. Kuzumi, A., Norimatsu, Y. & Matsuda, K. M. Comprehensive autoantibody pro
426 fi ling in systemic autoimmunity by a highly- sensitive multiplex protein array.
427 1–14 (2023) doi:10.3389/fimmu.2023.1255540.

- 428 46. Lunardi, C. *et al.* Systemic sclerosis immunoglobulin G autoantibodies bind the
429 human cytomegalovirus late protein UL94 and induce apoptosis in human
430 endothelial cells. *Nat. Med.* **6**, 1183–1186 (2000).
- 431 47. Ohtsuka, T. & Yamazaki, S. Increased prevalence of human parvovirus B19
432 DNA in systemic sclerosis skin. *Br. J. Dermatol.* **150**, 1091–1095 (2004).
- 433 48. Ho, D., Imai, K., King, G. & Stuart, E. A. MatchIt: Nonparametric Preprocessing
434 for Parametric Causal Inference. *J. Stat. Softw.* **42**, 1–28 (2011).
- 435 49. Khanna, D. *et al.* Standardization of the modified Rodnan skin score for use in
436 clinical trials of systemic sclerosis. *J. Scleroderma Relat. Disord.* **2**, 11–8 (2017).
- 437 50. Khanna, D. *et al.* Minimally important difference in diffuse systemic sclerosis:
438 results from the D-penicillamine study. *Ann. Rheum. Dis.* **65**, 1325–1329 (2006).
- 439
- 440

441 **Acknowledgements**

442 We thank Ms. Maiko Enomoto and her colleagues for their secretarial work.

443 We appreciate K. Yamaguchi, T. Okumura, C. Ono, A. Sato, A. Miya, and N. Goshima

444 from ProteoBridge Corporation for preparing the WPAs. We also acknowledge R.

445 Uchino, Y. Murakami, and H. Matsunaka from TOKIWA Pharmaceuticals Co. Ltd. for

446 providing technical assistance with autoantibody measurement.

447 **Author Contributions**

448 KM Matsuda primarily engaged in autoantibody measurement, clinical data
449 collection, data analysis, visualization, and writing the first draft of the manuscript. K
450 Iwadoh participated in machine learning analysis. S Ebata was primarily engaged in the
451 management of SSc patients participated in the DESIRES trial. H Kotani, A Kuzumi, T
452 Fukasawa, A Yoshizaki-Ogawa took part in the sample collection of SSc. S Sato
453 conceptualized and supervised the study. A Yoshizaki conceptualized, launched, and
454 supervised this study, and was involved in revising the manuscript.
455

456 **Conflict-of-interest statement**

457 T Fukasawa and A Yoshizaki belong to the Social Cooperation Program,
458 Department of Clinical Cannabinoid Research, The University of Tokyo Graduate
459 School of Medicine, Tokyo, Japan, supported by Japan Cosmetic Association and Japan
460 Federation of Medium and Small Enterprise Organizations. The remaining authors
461 declare that the research was conducted in the absence of any commercial or financial
462 relationships that could be construed as a potential conflict of interest.
463

464 **Materials and Methods**

465 *Study Design*

466 The study design for the DESIRES trial has been previously reported
467 (NCT04274257).¹³ Briefly, the DESIRES trial was a randomized, double-blind,
468 placebo-controlled trial of 24 weeks. In total, 56 patients were randomized to receive
469 either intravenous rituximab (375 mg/m²) or matching placebo once per week for 4
470 weeks. Of these, 49 patients completed the double-blind phase. Serum samples were
471 collected and served for PWAS at the beginning and the end of the double-blind phase
472 (**Fig. 1A**). After excluding 4 cases due to their serum unsuitable for PWAS, data of 45
473 patients were included in our analysis. Age and sex matched HCs were selected from a
474 cohort of healthcare providers on annual checkups without any medical history (**Fig.**
475 **1B**), using “matchIt” R package.⁴⁸ This study was approved by the ethics committee of
476 the University of Tokyo Graduate School of Medicine and conducted in accordance
477 with the Declaration of Helsinki. Written informed consent was obtained from all
478 patients.

479

480 *Assessments*

481 Clinical and laboratory assessments were performed at baseline and at 24
482 weeks after the first infusion of rituximab. Skin sclerosis was assessed by mRSS.⁴⁹
483 Lung function was evaluated by pulmonary function tests. Serum levels of Krebs von
484 den Lungen-6 (KL-6; normal range: 0-500 U/mL) and surfactant protein-D (SP-D;
485 normal range: 0-110 ng/mL), which are glycoproteins mainly produced by type II
486 pneumocytes, were measured as established markers of ILD in patients with SSc.
487 Laboratory examinations included white blood cell count, lymphocyte count, the
488 number of CD19⁺ and CD20⁺ cells, and serum levels of IgG (normal range: 700-1600
489 mg/dL), IgM (normal range: 40-250 mg/dL), and IgA (normal range: 70-400 mg/dL).
490 Patients with mRSS improvement of 7 or higher and 6 or lower were classified as HRs
491 and LRs, respectively, based on the previous study on minimally important differences
492 for mRSS.⁵⁰ This classification resulted in 16 high responders and 13 LRs (**Fig. 1C**).

493

494 *Autoantibody measurement*

495 WPAs were arranged as previously described.²⁰ First, proteins were
496 synthesized *in vitro* utilizing a wheat germ cell-free system from 13,455 clones of the
497 HuPEX.¹⁸ Second, synthesized proteins were plotted onto glass plates (Matsunami
498 Glass, Osaka, Japan) in an array format by the affinity between the GST-tag added to

499 the N-terminus of each protein and glutathione modified on the plates. The WPAs were
500 treated with human serum diluted by 3:1000 in the reaction buffer containing 1x
501 Synthetic block (Invitrogen), phosphate-buffered saline (PBS), and 0.1% Tween 20.
502 Next, the WPAs were washed, and goat anti-Human IgG (H+L) Alexa Flour 647
503 conjugate (Thermo Fisher Scientific, San Jose, CA, USA) diluted 1000-fold was added
504 to the WPAs and reacted for 1 hour at room temperature. Finally, the WPAs were
505 washed, air-dried, and fluorescent images were acquired using a fluorescence imager
506 (Typhoon FLA 9500, Cytiva, Marlborough, MA, USA). Fluorescence images were
507 analyzed to quantify serum levels of autoantibodies targeting each antigen, following
508 the formula shown below:

509

$$Autoantibody\ level\ [AU] = \frac{F_{autoantigen} - F_{negative\ control}}{F_{positive\ control} - F_{negative\ control}} \times 100$$

510 *AU*: arbitrary unit

511 $F_{autoantigen}$: fluorescent intensity of autoantigen spot

512 $F_{negative\ control}$: fluorescent intensity of negative control spot

513 $F_{positive\ control}$: fluorescent intensity of positive control spot

514

515 *Machine learning*

516 We applied supervised machine learning techniques using the Python code
517 with the scikit-learn library to analyze the autoantibody measurement data. With the
518 random forest model, decision trees were built and trained in parallel on subsets of
519 sampled instances and features. Meanwhile, with the XGBoost model, decision trees
520 were built sequentially to improve each other. The final prediction of the random forest
521 was based on the majority of its decision trees, while that of XGBoost was derived from
522 their weighted average. The performance of the classifiers was evaluated using the area
523 under the operator-receiver characteristics curve (AUC), accuracy, precision, recall, and
524 F1-score, with the higher the scores indicating the better classification performance. The
525 accuracy is the ratio of the correct positive and negative prediction, the precision is the
526 ratio of the correct positive prediction, the recall (or sensitivity) is the ratio of the
527 correct positive prediction among all true positive instances, and F1-score is the
528 harmonic mean of precision and sensitivity.

529

530 *WGCNA analysis*

531 The weighted gene co-expression network was constructed using the
532 "WGCNA" R package.²⁸ We calculated each gene pair's Pearson correlation coefficient,
533 measured how similarly their expressions were expressed, and created a correlation

534 matrix. Scale-free topology requirements were used to compute the "soft" threshold
535 power to build biologically meaningful scale-free networks. Based on the adjacency
536 matrix, dynamic tree cuts and at least 100 genes per module were utilized to generate a
537 topological overlap matrix for co-expression modules. In addition, we assessed gene
538 significance, module membership, and correlated modules with clinical characteristics
539 and mapped signature genes.

540

541 *Statistical analysis*

542 Fisher exact test was performed to compare categorical variables.
543 Mann-Whitney U test or Wilcoxon signed-rank test as appropriate was performed to
544 compare continuous variables. Spearman correlation test was used for correlation
545 analysis. P values of $<.05$ were considered statistically significant. Gene Ontology
546 Analysis using web-based tools targeted the list of the entry clones coding the
547 differentially highlighted autoantigens was performed for gene-list enrichment analysis,
548 gene-disease association analysis, and transcriptional regulatory network analysis with
549 Metascape.²⁵ Data analyses were conducted using R (v4.2.1).

550

551 *Data visualization*

552 Box plots, scatter plots, hierarchical clustering, and correlation matrix were
553 visualized by using R (v4.2.1). Box plots were defined as follows: the middle line
554 corresponds to the median; the lower and upper hinges correspond to the first and third
555 quartiles; the upper whisker extends from the hinge to the largest value no further than
556 1.5 times the interquartile range (IQR) from the hinge; and the lower whisker extends
557 from the hinge to the smallest value at most 1.5 times the IQR of the hinge.
558

Figure legends

Figure 1. Overview of the study. (A) The study design of the DESIRES trial. (B) The flow chart of sample acquisition in the present study. (C) The sum of autoantibody levels (SAL) in SSc at the baseline and HCs. (D) Absolute change of mRSS in SSc patients during the DESIREs trial. HR: high responder, LR: low responder. (E) SAL before and after the study period of the DESIRES trial by the treatment arm. (F) Serum levels of SSc-related autoantibodies before and after the study period of the DESIRES trial by the treatment arm. ATA: anti-topoisomerase I antibody, ACA: anti-centromere antibody, ARA: anti-RNA polymerase III antibody. *: $P < 0.05$, ****: $P < 0.0001$, NS: $P > 0.05$. P values were calculated by Mann-Whitney's U test.

Figure 2. Selection of autoantibodies of clinical relevance.

(A) Volcano plot that shows autoantibodies differentially elevated in SSc before treatment compared to HCs. The vertical dash line indicates $P = 0.05$. (B) Volcano plot that shows autoantibodies differentially increased in HRs than in LRs. (C) Volcano plot that shows autoantibodies significantly reduced in HRs during RTX therapy. (D) Heat map that shows the serum levels of 58 candidate autoantibodies of clinical relevance. (E) Principal component analysis of 58 candidate autoantibodies of clinical relevance. In the scatter plot, individual subjects as points. The loading diagram illustrates the contributions to PC1 and PC2. (F) SAL focused on 58 candidate autoantibodies of clinical relevance. ***: $P < 0.001$, ****: $P < 0.0001$, NS: $P > 0.05$. P values were calculated by Mann-Whitney's U test. (G) The receiver-operator characteristics (ROC) curve demonstrating the discrimination between SSc and HCs by all the measured autoantibodies (green) and by 58 candidate autoantibodies of clinical relevance (yellow). (H) The ROC curve demonstrating the discrimination between HRs and LRs by all the measured autoantibodies (green) and by 58 candidate autoantibodies of clinical relevance (yellow).

Figure 3. Proteins targeted by the candidate autoantibodies of clinical relevance.

(A) Gene ontology analysis encompassing the genes coding proteins targeted the candidate autoantibodies. (B) The circos plot represents the inclusion relationship between each gene ontology and the candidate autoantibodies. (C) Serum levels of candidate autoantibodies associated with “import across plasma membrane.” (D) The heatmap illustrates correlation between the candidate autoantibodies associated with “import across plasma membrane” and clinical traits of SSc. (E) Serum levels of autoantibodies associated with “peptide GPCRs.” (F) The heatmap illustrates correlation between the candidate autoantibodies associated with “peptide GPCRs” and clinical traits of SSc. *: $P < 0.05$, **: $P < 0.01$, ***: $P < 0.001$. P values were calculated by Spearman’s correlation test.

Figure 4. WGCNA analysis. (A) Network heatmap plot. Branches in the hierarchical clustering dendrograms correspond to modules. Color-coded module membership is displayed in the color bars below and to the right of the dendrograms. In the heatmap, high co-expression interconnectedness is indicated by progressively more saturated yellow and red colors. (B) Gene ontology analysis encompassing the genes coding proteins targeted by autoantibodies included in the “turquoise,” “darkmagenta,” and “tan” modules. (C) The heat map illustrates correlation between each module identified by WGCNA analysis and clinical traits of SSc. (D) The heatmap shows the correlation between each module and clinical trait. *: $P < 0.05$, **: $P < 0.01$, ***: $P < 0.001$, ****: $P < 0.0001$. P values were calculated by Spearman’s correlation test.

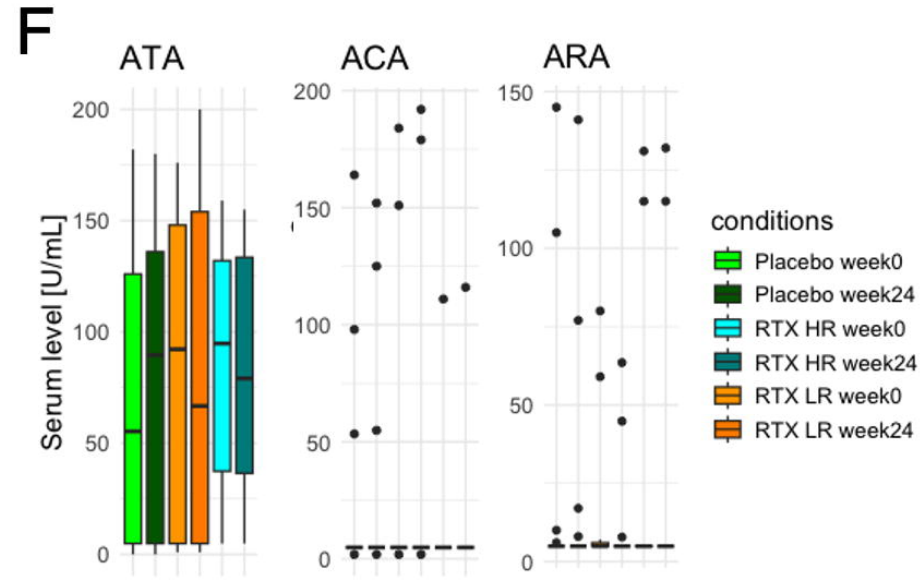
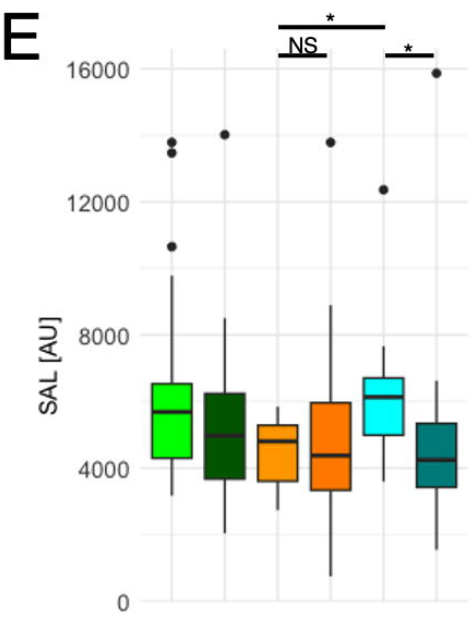
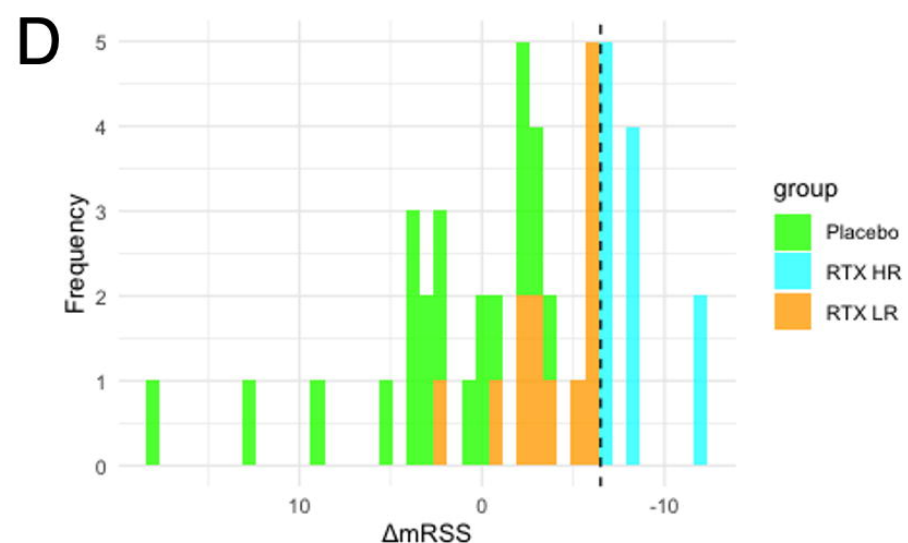
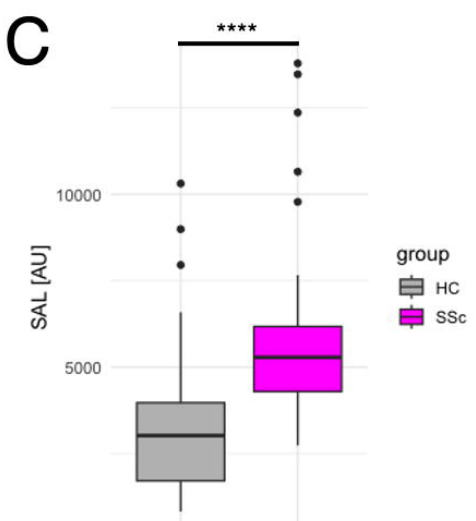
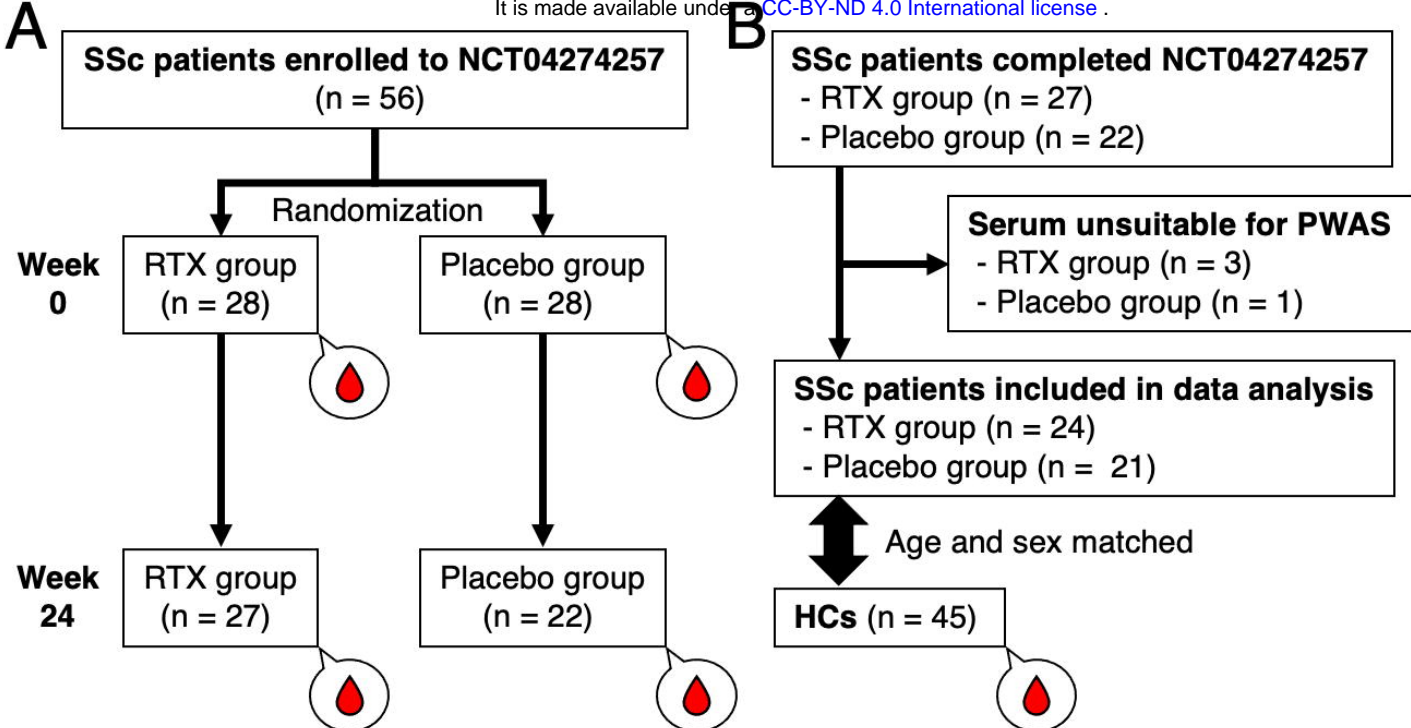
Extended Figure 1. Additional results of PWAS. (A) The sum of autoantibody levels (SAL) by age groups. (B) Serum levels of SSc-related autoantibodies before and after the DESIRES trial by the treatment arm and responsiveness.

Extended Figure 2. Autoantibodies highlighted in each machine learning model.

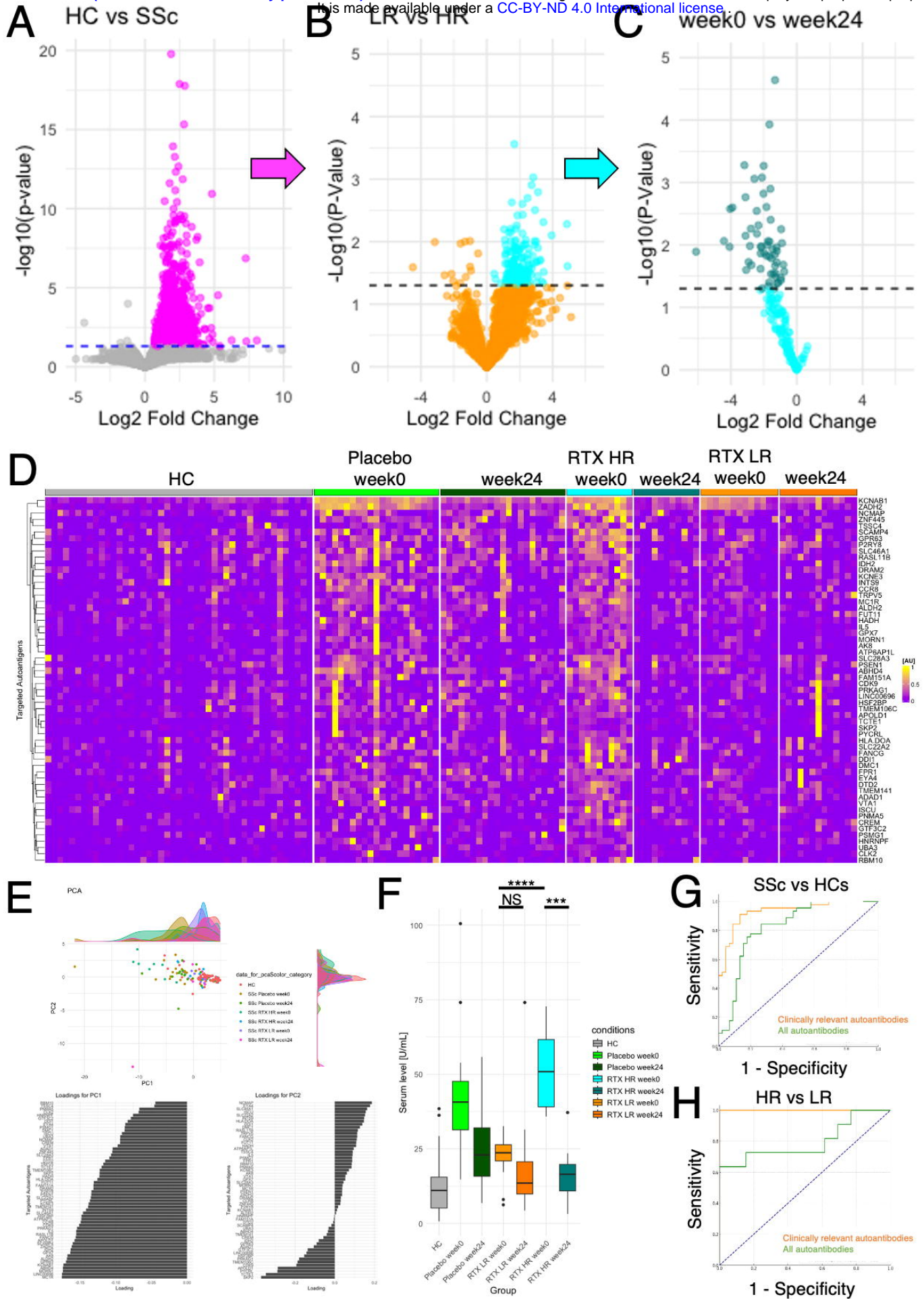
(A) Autoantibodies that were mostly highlighted according to feature importance by Lasso regression, Ridge regression, SVM with normalization, Random Forest, XGBoost, and LightGBM. (B) The inclusion relationship of autoantibodies highlighted by the six machine learning frameworks illustrated by an UpSet plot. (C) The box plots describe the serum levels of autoantibodies highlighted by more than two frameworks in COVID-19, atopic dermatitis (AD), anti-neutrophil cytoplasmic antibody-associated vasculitis (AAV), systemic lupus erythematosus (SLE), systemic sclerosis (SSc), and healthy controls (HCs). The data derives from the UT-ABCD.

Extended Figure 3. Distribution of the candidate autoantibodies among various disorders. The box plots describe the serum levels of the candidate autoantibodies associated with “import across plasma membrane” (**A**) and “peptide GPCRs” (**B**) in COVID-19, atopic dermatitis (AD), anti-neutrophil cytoplasmic antibody-associated vasculitis (AAV), systemic lupus erythematosus (SLE), systemic sclerosis (SSc), and healthy controls (HCs). The data derives from the UT-ABCD.

Extended Figure 4. Expression of highlighted autoantigens in human tissues and single cells. Expression of autoantigens associated with “import across plasma membrane” (**A**) or with “peptide GPCRs” (**B**) in multiple human tissues, as measured by bulk RNA-sequencing from the Human Protein Atlas. Expression of CCR8 (**C**) or FPR1 (**D**) in immune cells from multiple human tissues, as measured by single-cell RNA-sequencing from the Tabula Sapiens project.



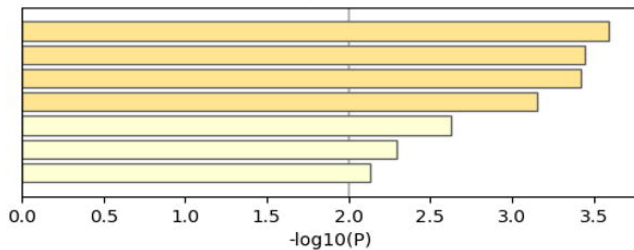
Matsuda KM et al.
Figure 1



Matsuda KM et al.
Figure 2

A

Gene Ontology Analysis

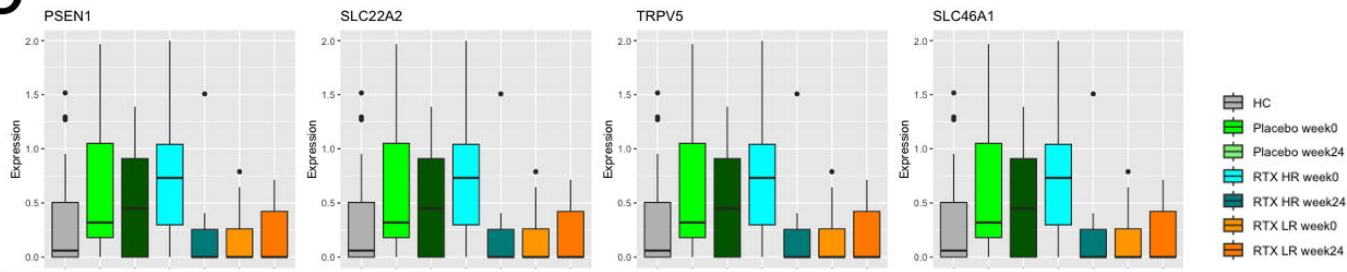


GO:0098739: import across plasma membrane
 WP24: Peptide GPCRs
 GO:0006281: DNA repair
 GO:1904063: negative regulation of cation transmembrane transport
 GO:0043467: regulation of generation of precursor metabolites and energy
 GO:0043484: regulation of RNA splicing
 R-HSA-112316: Neuronal System

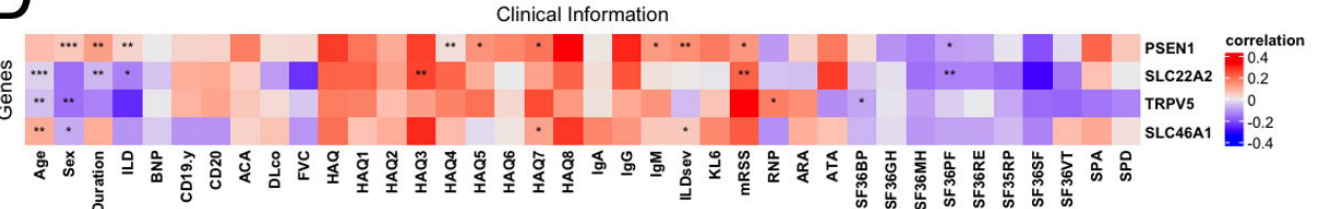
B

	PSEN1	SLC22A2	TRPV5	SLC46A1	CCR8	FPR1	MC1R	GPR63
GO:0098739	Red	Red	Red	Red				
WP24					Red	Red	Red	Red
GO:0006281							Red	
GO:1904063								
GO:0043467	Red							
GO:0043484								
R-HSA-112316		Red						

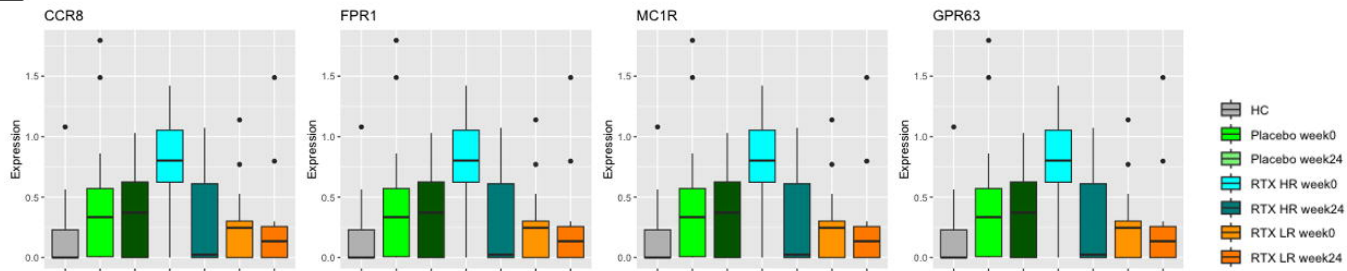
C



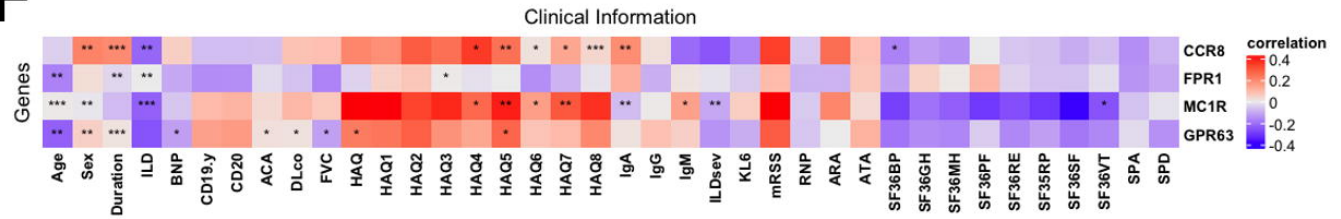
D



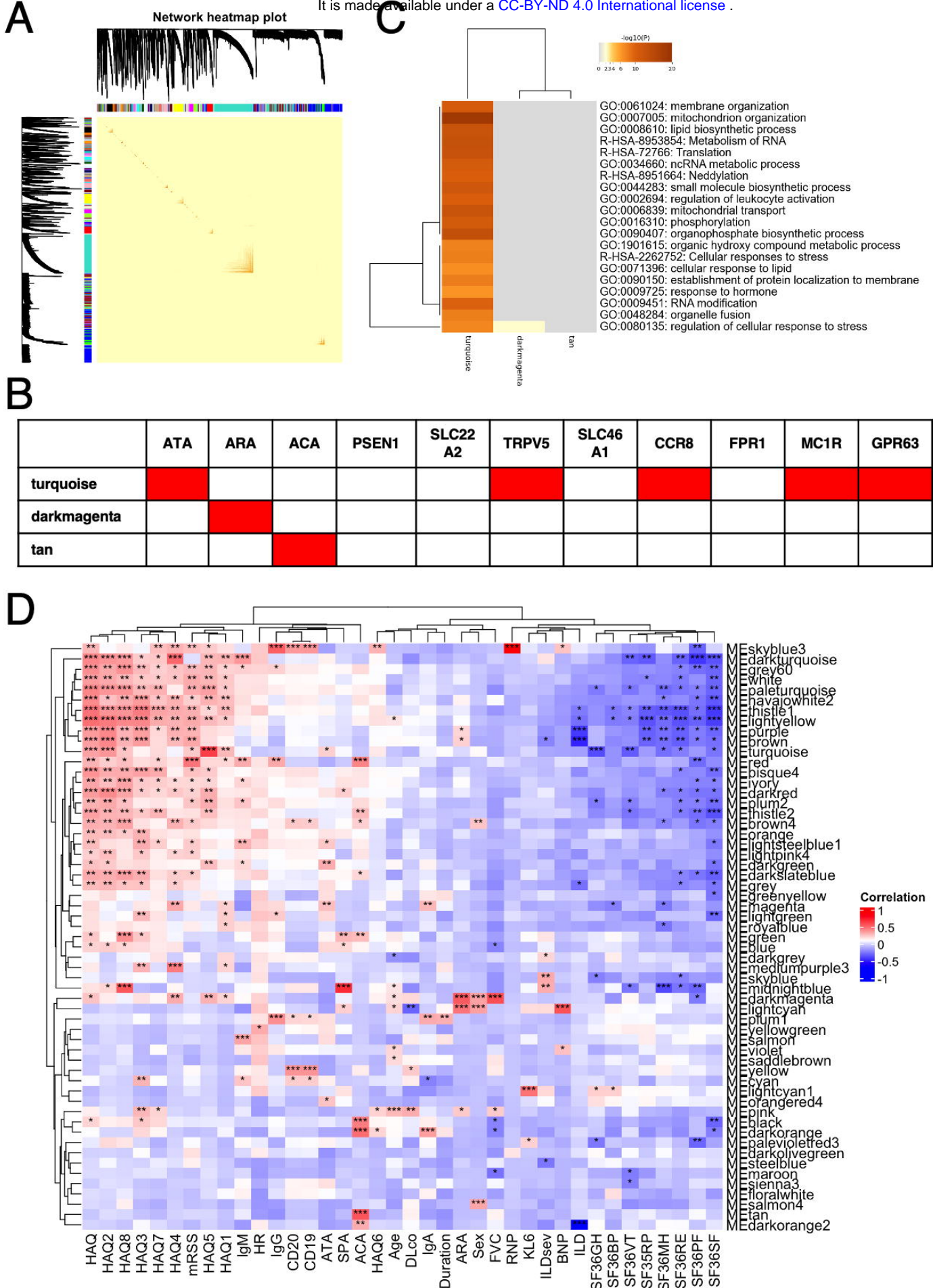
E



F



Matsuda KM et al.
 Figure 3



Matsuda KM et al.
 Figure 4